DOUBLE FIT: Optimization procedure applied to lattice strain model

Célia Dalou, Julien Boulon, Kenneth T. Koga, Robert Dalou, Robert Dennen

Accepted Manuscript

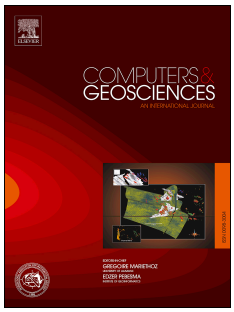

DOUBLE FIT: Optimization procedure applied to lattice strain model

Celia Dalou, Julien Boulon, Kenneth T. Koga, Robert Dalou, Robert Dennen

PII: S0098-3004(17)31178-0

DOI: 10.1016/j.cageo.2018.04.013

Reference: CAGEO 4125

To appear in: *Computers and Geosciences*

Received Date: 15 November 2017

Revised Date: 19 March 2018

Accepted Date: 30 April 2018

Please cite this article as: Dalou, C., Boulon, J., T. Koga, K., Dalou, R., Dennen, R., DOUBLE FIT: Optimization procedure applied to lattice strain model, *Computers and Geosciences* (2018), doi: 10.1016/j.cageo.2018.04.013.

DOUBLE FIT: Optimization procedure applied to lattice strain model

Celia Dalou*1, Julien Boulon2, Kenneth T. Koga3, Robert Dalou4, Robert Dennen5

1. Celia Dalou, PhD
Affiliation: CNRS - CPRG, Centre de Recherches Pétrographiques et Géochimiques, UMR 7358 CNRS-UL
Address:15 rue Notre Dame des Pauvres, BP 20, 54501 Vandoeuvre-lès-Nancy, France
Phone number: +33-3-83-51-17-98
* corresponding author : cdalou@crpg.cnrs-nancy.fr

2. Julien Boulon, PhD
Affiliation: LCAR – Laboratoire Collisions, Agrégats, Réactivité – UMR5589
Address: Université Paul Sabatier – Bât. 3R1b4,
118, route de Narbonne, 31062 Toulouse Cedex 09, France

3. Kenneth T. Koga, PhD
Affiliation: Laboratoire Magmas et Volcans, Université Clermont Auvergne - CNRS - IRD, OPGC
Address: 6 Avenue Blaise Pascal, 63178 Aubière, France

4. Robert Dalou,
Retired
Address: private

5. Robert Llewellyn Dennen, Master
Affiliation: Self-employed, RD Geoscience Editing
Address: private

Authorship statement

CD designed the DOUBLE FIT program and wrote the paper, JB wrote the original python code to adapt the differential evolutionary algorithm (Storn and Price, 1997) to the lattice strain model, KK implemented weighted fit and uncertainty propagation, R. Dalou programmed and designed the user-interface, and R. Dennen helped design the user-interface and the figures on the paper.

Abstract

Modeling trace element partition coefficients using the lattice strain model is a powerful tool for understanding the effects of *P-T* conditions and mineral and melt compositions on partition coefficients, thus significantly advancing the geochemical studies of trace element distributions in nature. In this model, partition coefficients describe the strain caused by a volume change upon cation substitution in the crystal lattice. In some mantle minerals, divalent, trivalent, and tetravalent trace element cations are mainly substituted in one specific site. Lattice strain model parameters, for instance in olivine and plagioclase, are thus fit for one crystal site. However, trace element cations can be substituted in two sites in the cases of pyroxenes, garnets, amphiboles, micas, or epidote-group minerals.

To thoroughly study element partitioning in those minerals, one must consider the lattice strain parameters of the two sites. In this paper, we present a user-friendly executable program, working on PC, Linux, and Macintosh, to fit a lattice strain model by an error-weighted differential-evolution-constrained algorithm (Storn, R., and Price, K. 1997. Differential evolution - A simple and efficient heuristic for global optimization over continuous spaces. Journal of Global Optimization 11, 341-359). This optimization procedure is called DOUBLE FIT and is available for download on http://celiadalou.wixsite.com/website/double-fit-program. DOUBLE FIT generates single or double parabolas fitting experimentally determined trace element partition coefficients using a very limited amount of data (at minimum six experimental data points) and accounting for data uncertainties. It is the fastest calculation available to obtain the best-fit lattice strain parameters while accounting for the elastic response of two different sites to trace element substitution in various minerals.

Keywords: trace elements, partition coefficients, pyroxenes, lattice strain, fitting

1. Introduction

Elemental partition coefficients between Earth's phases are commonly employed to

interpret geochemical signatures of mantle-derived igneous melts and rocks. Because trace element partitioning between equilibrated minerals an melts strongly depends on their chemical compositions and the melting or crystallization pressure (*P*) and temperature (*T*) conditions, trace element abundances in magmas can constrain the depth, temperature, and extent of their partial melting in the mantle (e.g. Wood and Blundy, 1997; Wood et al., 1999; van Westrenen et al., 1999; Hill et al., 2000; van Westrenen et al., 2000a,b; Salters et al., 2002; Bédard, 2007; Frei et al., 2009; van Kan Parker et al., 2010; Dalou et al., 2009, 2012; Cartier et al., 2014; Dygert et al., 2014; Bobrov et al., 2014; Michely et al., 2017). Therefore, partition coefficients (*D*) cannot be used as fixed values in geochemical models, and understanding their variation with *P*-*T* conditions and mineral and melt compositions is fundamental.

To do so, results of trace element partitioning studies are interpreted within the framework of the lattice strain model (Blundy and Wood, 1994), which describes the substitution parameters of elements in different crystal sites. In mantle minerals such as olivine or plagioclase, divalent, trivalent, and tetravalent trace element cations are mainly substituted in one site, respectively the M2 and M octahedral sites (Wood and Blundy, 2007). Lattice strain model parameters for those minerals are thus fitted for one crystal site (M2 in olivine, e.g. Beattie, 1994; Taura et al., 1998; Zanetti et al., 2004; Lee et al., 2007; Michely et al., 2017; or M in plagioclase, e.g. Blundy and Wood, 1991; Bindeman et al., 1998; Tepley et al., 2010; Sun et al., 2017). In contrast, trace element cations can be substituted in both the M1 and M2 octahedral sites of pyroxenes and tri-octahedral micas such as phlogopite and biotite, in the dodecahedral X site and the octahedral Y site in garnet (sometimes possibly into its T site), in the three octahedral sites (M1, M2, and M3), the distorted cubic M4 site, and the distorted cuboctahedral site A in amphiboles (Wood and Blundy, 2007; Sun et al., 2018), and the 7- to 11-fold coordinated A1 and A2 sites in epidote-group minerals (Frei et al., 2003). Nevertheless, in many pyroxene-melt partitioning studies (orthopyroxene, e.g. Green et al., 2000; Bédard, 2007, Lee et al., 2007; and clinopyroxene, e.g. Hill et al., 2000; Adam and Green, 2003, 2006; Gaetani et al., 2003; McDade et al., 2003a,b; Bédard et al., 2014; Michely et al., 2017), cations in the M1 site are not accounted for in the lattice strain model. Similarly, the lattice strain model is often applied only to the X site in garnets (e.g. van Westrenen et al., 1999,

2000b; Green et al., 2000; Klemme et al., 2002; Adam and Green, 2003, 2006; Gaetani et al., 2003; Pertermann et al., 2004; Corgne et al., 2004; Dalou et al., 2009). Others consider multiple sites, but fit them separately in the lattice strain model (e.g. Adam and Green, 2003, 2006; Dygert et al., 2014 for pyroxenes; Brenan et al., 1995; La Tourrette et al., 1995; Dalpé and Baker, 2000 for amphiboles and phlogopites; and Frei et al., 2003 for epidote-group minerals), overlooking a possible relationship between the elastic parameters of the two sites.

To apply the lattice strain model to both sites and fit experimentally determined trace element partition coefficients, several approaches have been proposed. Frei et al. (2009) and van Kan Parker et al. (2010) fit their experimental values using a weighted nonlinear least square Levenberg-Marquardt routine using the observed $D_i^{\text{opx-melt}}$ as a weighting factor, and minimizing $\chi^2 = \Sigma[(D_i^{\text{observed}} - D_i^{\text{calculated}})^2/D_i^{\text{observed}}]$ (Press et al., 1992). This method is limited as it is partly fitted by fixing some parameters. Cartier et al. (2014) opted for a Monte Carlo-type approach; this brute-force method is more robust but requires a large number of data and/or a long calculation time. In addition, both methods did not account for data uncertainties.

In this paper, we present DOUBLE FIT, a lattice strain model fit by a differential-evolution-constrained algorithm (Storn and Price, 1997) adapted to be error weighted. The optimization procedure generates double pseudo-parabolas fitting experimentally determined trace element partition coefficients using a very limited amount of data (at minimum 6 experimental data points, Fig. 1), is the first lattice-strain fitting program accounting for measurement errors on data points, and offers the fastest calculation of the best-fit values for the lattice strain parameters of both pyroxene sites: r_0^{M1}, r_0^{M2}, E^{M1}, E^{M2}, D_0^{M1}, and D_0^{M2}.

2. Lattice strain models for pyroxenes

At equilibrium, the dependence of trace element partitioning on the mineral composition attests to changes in the crystal structure (e.g. Blundy and Wood, 1994; see also the review by Blundy and Wood, 2003) when considering the crystal structure as an elastic body (Nagasawa, 1966; Brice, 1975). Substitution of a trace element cation for an

essential structural constituent of a crystal affects the lattice energetics of crystallographic sites due to the misfit between the substituted cation and the essential structural constituent whose radius is very close to the ideal radius of the site (Nagasawa, 1966; Brice, 1975; Beattie, 1994; Blundy and Wood, 1994; Wood and Blundy, 1997). According to their ionic radius and charge, elements are incorporated into different crystal sites. Each site is characterized by the parameters of the lattice strain model (Brice, 1975; Blundy and Wood, 1994). This model is based on the observation of a pseudo-parabolic relationship between cationic radii, r_i, and $\ln(D_i^{\text{crystal/melt}})$ values for isovalent trace elements, i (Onuma et al., 1968), in which $D_i^{\text{crystal/melt}}$ is the Nernst partition coefficient based on concentration ratios. This model, applied to the two pyroxene structural sites, is characterized by six parameters: r_0^{M1} and r_0^{M2}, the ideal (strain-free) radii of the M1 and M2 sites, respectively; E^{M1} and E^{M2}, the elastic response of the sites to the elastic strain caused by r_i different than r_0^{M1} and r_0^{M2}; and D_0^{M1} and D_0^{M2}, the fictive strain-free partition coefficients for the cations with r_0^{M1} and r_0^{M2}, respectively. Following Frei et al. (2009), $D_i^{\text{crystal/melt}}$ regression to the lattice strain model is expressed as:

$$D_i^{crystal/melt} = D_o^{M1} \exp\left(\frac{\alpha \cdot E^{M1}}{T}\left(\frac{r_0^{M1}}{2}(r_i - r_0^{M1})^2 + \frac{1}{3}(r_i - r_0^{M1})^3\right)\right) + D_o^{M2} \exp\left(\frac{\alpha \cdot E^{M2}}{T}\left(\frac{r_0^{M2}}{2}(r_i - r_0^{M2})^2 + \frac{1}{3}(r_i - r_0^{M2})^3\right)\right) \quad (1)$$

where T is temperature in Kelvin and $\alpha = \frac{-4\pi N_a}{R}$ with N_a the Avogadro constant and R the gas constant.

3. Algorithms used to resolve the lattice strain models for 2 crystal sites

3.1 Previous work

Previous works have used the nonlinear least square Levenberg-Marquardt algorithm (Frei et al., 2009; van Kan Parker et al., 2010). The Levenberg-Marquardt method often works well for nonlinear problems because they are guided by the geometry

of the objective function (e.g. the least square sum) in parameter space. However, in many cases, this objective function may present many local minima. When there are numerous minima, the algorithm becomes trapped in the first that it encounters. Therefore, such algorithms are very sensitive to the initial set of parameters, which must be very close to the optimized values if local minima are present.

The Monte-Carlo method, as used by Cartier et al. (2014), randomly generates a large number of possible solutions within a predefined range of lattice parameters. The best solutions are selected according to the deviation from experimental data. To limit the number of solutions and therefore the calculation, the solution domain (i.e. the range of parameters) must be restricted, either using literature data or "by eye" using experimental data for r_0^{M1}, r_0^{M2}, D_0^{M1}, and D_0^{M2}.

During global minimization, these methods are susceptible to failure in relatively poorly-constrained situations, such as a minimization of six parameters with relatively few data constraints. This is illustrated by mapping the residual surface of the systematic variation of r_0^{M1}, r_0^{M2}, E^{M1}, and E^{M2} to calculate D_0^{M1} and D_0^{M2} by simple matrix inversion. Figure 2 is a contour plot of the uncertainty-weighted residual square surface of E^{M2} versus r_0^{M2}, showing isolated local minima near the global minimum and a gradient change at around $r_0^{M2} = 0.9$. Furthermore, we noted significant shifts of global minima depending on the mapping resolution. These hidden issues of parameter fitting lead to the publication of datasets that are often difficult to reconcile.

A solution to minimize these numerical problems is to use a global optimization procedure, which explores a very large portion of the objective function landscape when searching for the global minimum.

3.2. Differential-evolution-constrained algorithm

Compared to more classical "random search" methods, evolutionary algorithms (a form of global optimization) can be considered as "guided random search" algorithms. They are known as "evolutionary" because they take inspiration from natural evolution concepts like survival of the fittest, crossover, and mutation. In other words, more classical optimization methods consider a single best solution, whereas evolutionary

algorithms consider a population of candidate solutions; within that population, one candidate is the best, but the others are kept as "samples" from which a better solution can be found later. Therefore, evolutionary algorithms cannot be trapped at local optima when a better solution can be found far from the current solution. Evolutionary methods are thus extremely robust: they have an increased chance of finding a global or near global optimum, are easy to implement, and are well suited for discrete optimization problems. In the case of the lattice strain model, the global minimum must comply with crystallographic requirements; therefore, crystallographic boundary conditions are applied, reducing the parameter space.

Among the evolutionary methods, the differential evolutionary method is a stochastic direct search method, which optimizes problems by iteratively trying to improve a candidate solution based on a given quality criterion. This method has the advantage of being easily "applied to experimental minimization where the cost value is derived from a physical experiment" (Storn and Price, 1997). Applied to the lattice strain model as the objective function $\mathcal{O}(\mathbf{p})$ (Eq. 1), we consider an experimental data set, accounting for uncertainties on the data, here one standard deviation of a set of measurements, with N measured points $\mathcal{E}(r_i, D_i^{X/Y})$, where r_i is the ionic radius of element i and $D_i^{X/Y}$ the partition coefficient between phases X and Y, with i = 1, 2,..., N. The modeled data set, $\mathcal{M} = D_i^{X/Y}(r_j, \mathbf{p})$, is computed assuming a lattice strain model with n continuous adjustable parameters $\mathbf{p} = \{p_1, p_2,..., p_n\}$. The simulated data set $\mathcal{M}$ is then compared to $\mathcal{E}$ using the objective function $\mathcal{O}(\mathbf{p})$. The differential evolution algorithm will attempt to find the optimal vector $\mathbf{p}$ guided by $\mathcal{O}(\mathbf{p})$, starting with an initial population of randomly generated parameter vectors which evolve during mutation, cross-over, and selection cycles (Fig. 3), by minimizing two cost functions using the Nash criterion (>0.9995) and the root mean square error (RMSE < 0.03). This evolution reduces calculation time and can adapt to a very limited number of input experimental data.

The DOUBLE FIT program can fit the lattice strain model with as few as six experimental $D_i^{px/melt}$ values, and calculates the six model parameters. This is possible because DOUBLE FIT accounts for the associated (and non-equal) errors on the data

values. Analytical constraints (interferences, analysis time, measurement accuracy) or the chemical system itself (e.g. the number of divalent and tetravalent cations is generally limited) often limit petrologists to selecting a limited number of elements to analyze, and thus a limited number of partition coefficients to fit (e.g., Fig. 1). To allow calculation of standard deviations on each lattice parameter, the DOUBLE FIT optimization runs 50 times. Calculation times vary between 20 and 40 s depending on the number of experimental data and the chosen parameter ranges.

4. Description and use of the program

DOUBLE FIT is an executable program written in the Python programming language and transformed as an executable (.app) available for download at http://celiadalou.wixsite.com/website. DOUBLE FIT runs on PC (64 bits only), Linux, and Macintosh, requiring only spreadsheet software to create a .csv data file. The input data files and variables can be entered directly in user-friendly windows following a straightforward procedure. DOUBLE FIT is thus easily accessible for users with no prior coding experience.

DOUBLE FIT provides four options:

- two options for a single fit procedure (one pseudo-parabola), for use with minerals where trace elements substitute in mainly one site (i.e. olivine and plagioclase), and
- two options for a double fit procedure applied to minerals where trace elements can substitute in two sites (i.e. pyroxene, garnet, micas, and epidote-group minerals).

For either the single or double fits, the program calculates the best-fit parameters based on the experimental data, and plots pseudo-parabolas. Published lattice strain parameters and partition coefficients can be specified for both the single and double fits to plot the pseudo-parabolas with the same formatting as figures output by the DOUBLE FIT optimization program. This option facilitates comparison between the DOUBLE FIT optimization and literature data.

255 *4.1. Input data files*

256

257 Experimental data are called from a .csv file as presented in Figure 4. Individual
258 files must be created for divalent, trivalent, and tetravalent cations.

259 Cationic radii (first column, Ri) can be found in Shannon (1976) accounting for
260 the coordination of the substitution site of the studied mineral. For instance, as shown in
261 Figure 4 for trivalent cations, cations in orthopyroxene are in 6-fold coordination in both
262 octahedral sites, while in clinopyroxene, they are in 6-fold coordination in the M1 site
263 and 8-fold coordination in the M2 site. When only one substitution site is considered (e.g.
264 only Sc and rare earth elements, REE, are fitted for the trivalent cations), cations of
265 interest are 6-fold coordinated in the olivine M2 site, 8-fold coordinated in the garnet X
266 site or plagioclase A site, and 12-fold coordinated in the Ca-perovskite Ca site. However,
267 as cations can change coordination or substitution site depending on mineral composition
268 (e.g. Ba in amphiboles; Tiepolo et al., 2007) and/or their valence with oxygen fugacity
269 (e.g. Eu in plagioclase; Aigner-Torres et al., 2007; V, Cr, and Ti in pyroxenes; Cartier et
270 al., 2014), special attention should be paid when assigning ionic radii to each cation. For
271 instance, to determine the proportion of Eu^{2+} versus Eu^{3+}, i.e. to recalculate D_{Eu2+} and
272 D_{Eu3+}, Aigner-Torres et al. (2007) used a rearranged version of the lattice strain model
273 equation of Blundy and Wood (1994) in which D_0 and r_i are replaced respectively by the
274 measured partition coefficient and ionic radius of Sr to calculate D_{Eu2+} and of another
275 REE^{3+} (preferably Gd or Sm) for D_{Eu3+}, and $r_0^{(2+,3+)}$ and $E^{(2+,3+)}$ are fixed values taken
276 from Blundy and Wood (2003). This method allows fitting the recalculated D_{Eu2+} with
277 other divalent cations and the recalculated D_{Eu3+} with other trivalent cations.

278 The second column (D) of the data file corresponds to the measured partition
279 coefficients and the third column (eD) to their standard deviations. The minimum number
280 of data is six partition coefficients for the double fit options and three for the single fit
281 options. Although the fitting procedure works with these minimum numbers of data, if all
282 data are on the same side of the parabola, the fit will not reflect the true crystallographic
283 parameters. The ideal case to predict an accurate lattice strain model is to have data on
284 each side of the r_0 value in the case of the simple fit and on each side of the r_0^{M1} and r_0^{M2}
285 in the case of the double fit.

The data file must be saved in .csv format, using "." for decimals and ";" for separation between columns.

4.2 Procedure: example applied to clinopyroxene/melt partition coefficients

We recommend saving the DOUBLE FIT program (__DOUBLE_FIT_m or w64__ folder) and data test files within the same directory. Once the executable file is started, it opens a terminal window and asks for the input data file path (Supplementary Fig. S1a), defaulting to a Data_test/CPX_test.csv location provided as an example. The second window asks for the experimental temperature in degrees Celsius (Supplementary Fig. S1b).

The third window (Supplementary Fig. S1c) allows the user to enter known parameters or continue with the full optimization procedure. Parameters must be entered in the correct units: E in Pa and r_0 in m. This option simply offers the possibility to compare lattice strain parameters obtained via another method in the same graphic output as our program. To continue with the full optimization procedure, users should proceed without entering any parameters (leaving the fields blank). The fourth window asks for the valence of the trace element to be fitted (Supplementary Fig. S2a).

To reduce the possibility of multiple solutions (and the optimization time), we propose a range of the D_0^{M1}, D_0^{M2}, E^{M1}, E^{M2}, r_0^{M1}, and r_0^{M2} parameters within which the optimization procedure searches for the best-fit parameters; this default range appears in the fifth window (Supplementary Fig. S2b) and changes depending on the valence of the trace elements (see Cartier et al., 2014). To reduce or extend the parameter ranges (and thus run time), new minima and maxima can be entered in the fifth window. If no values are entered, the optimization will continue with the default parameter ranges.

The procedure presented above also applies to the single fit procedure for single-substitution-site minerals. For the single fit option, the input data file path defaults to a SData_test/OL_test.csv location provided as an example for olivine/melt partition coefficients of trivalent cations. Additional examples of the double fit option, including partition coefficients of trivalent cations for orthopyroxene, amphibole, and garnet, are available for download at the same location.

317

318 *4.3 Results*

319

320 After 20–40 s, results are available in the terminal (Supplementary Fig. S3a) and
321 in a results.txt file generated simultaneously. Graphical results are displayed another 2 s
322 later as a .png figure in a Python graphical window (Supplementary Fig. S3b). The figure
323 title includes the data file path and the run temperature of the sample. Best-fit parameters
324 with their standard deviations (after 50 iterations) are displayed on the figure. The figure
325 can be saved as .eps, .pdf, .ps, .svg, or .svgz for modification in vector graphical editors
326 for publication. Finally, users can continue using the same data file, select a new file, or
327 exit the program (Supplementary Fig. S3c) after closing the Python graphical window.

328

329 *4.4 Limitations*

330

331 The lattice strain parameters must be constrained to minimize the cost functions,
332 reduce run time, and avoid multiple convergence possibilities. We observe that when the
333 parameter space is left very large (e.g. D_0^{M1} and $D_0^{M2} \in [0.001 ; 100]$ and E^{M1} and $E^{M2} \in$
334 [100 ; 10000] GPa), statistical criteria are not satisfied, such as a subminimal Nash
335 criterion (<0.950), root mean square error (RMSE) >>1, errors on best-fit parameters
336 >100%, and/or a visually unsatisfactory fit.

337 Dalou et al. (2012) fit trivalent cations using the differential-evolution-constrained
338 algorithm (Storn and Price, 1997) via a primitive version of the DOUBLE FIT program,
339 and chose to minimize the cost functions using the Nash criterion (>0.9997) and RMSE <
340 0.04 while running the program in an acceptable time (maximum 30 s). To fulfill those
341 requirements, they constrained each parameter "with realistic boundary values"
342 (according to the accuracy of the measured data). The parameter space was defined to
343 avoid *a priori* determination (e.g. $E^{M2} \in [100 ; 1000]$ GPa). However, in a few cases
344 when data uncertainties were too significant, especially on La, they choose to decrease
345 the parameter space to allow convergence in a reasonable time (i.e. $E^{M2} \in [350 ; 430]$
346 GPa).

These limitations arise directly from the differential evolutionary algorithm, which does not guarantee that a best-fit solution can be found. Here, for instance, when standard deviations on one or more $D_i^{X/Y}$ (i.e. on the experimental data $\mathscr{E}(r_i, D_i^{X/Y})$) are too large, the algorithm cannot minimize the cost function according to the criteria chosen (Nash criterion > 0.9997 and RMSE < 0.04). When this occurs, users can either discard experimental data with large uncertainties or reduce the parameter space.

Another limitation is that, because DOUBLE FIT was designed to run over a large parameter space, no convergence is possible if, on more than one experimental datum, errors exceed the partition coefficient values (D < eD). This generally applies to the largest most-incompatible cations such as La and Ce, which are quite difficult to measure in pyroxenes as they are at very low concentrations and their measurements are easily contaminated by surrounding melt. In that case, it may be best to discard very incompatible cation data to fit the lattice strain model.

Whereas for trivalent cations, a large number of trace elements are measured, fewer, generally five or less, are typically measured for divalent (Ba, Pb, Sr, Ca, and Co) and tetravalent cations (Th, U, Zr, Hf, and Ti), and by extension mono- and pentavalent cations. This limitation can be overcome if the parameter space is reduced from the default range, as shown on Fig. 5a for tetravalent cations. The addition of Mg and Ni data in the M1 site allows using DOUBLE FIT for divalent cations (Fig. 5c). However, when errors are large, it might be best to consider individually fitting the M1 and M2 sites using the single fit option. For trivalent cations, the DOUBLE FIT program and the weighted non-linear least square Levenberg-Marquardt routine (Frei et al., 2009) result in equally good results (Fig. 5b).

5. Example of application: Search for chemical equilibrium among orthopyroxene partitioning experiments

Because most incompatible elements are concentrated in clinopyroxene rather than orthopyroxene, more mineral/melt partition coefficient data and lattice strain modeling are available for clinopyroxene than for orthopyroxene. One of the main reasons for this is the difficulty in accurately measuring low trace element concentrations

in orthopyroxene. Another limitation lies in the capabilities of measuring trace element concentrations in orthopyroxene not contaminated by melt, implying very large orthopyroxene or a very small analytical beam (sometimes <20 µm). The best example is La; the measured partition coefficient is often too large to represent the accurate La partition coefficient between mineral and melt (e.g. van Westrenen et al., 1999). In most cases, La is discarded from the dataset and not used to fit lattice strain models (Cartier et al., 2014).

One fundamental aspect of studying experimentally determined partition coefficients is the attainment of chemical equilibrium. For major elements, one can use textural observations (i.e. crystal shape), lack of compositional zoning in the crystal and heterogeneity in the melt pool, the value of Fe-Mg exchange coefficients between minerals and melts, or convergence of mass balance. For trace elements, most experimental petrologists use the lattice strain models, arguing that if their trace element partition coefficients can be plotted using the model then their partitioning data are near chemical equilibrium. We suggest using this argument with caution, especially when the experimental data are fitted with biases such as fixed parameters or narrow parameter spaces. As shown on Fig. 5, multiple possibilities exist depending on the size of the parameter space. This result is an outcome of any algorithm (not just DOUBLE FIT) applied to the lattice strain model for a given data set. Decisions regarding the size of the parameter space must be based on sound crystallographic knowledge to fully interpret the lattice strain model: although interpretation of the lattice strain model provides hints to partitioning data, it may not reflect equilibrium.

By calculating the energetics of ion substitution using atomistic simulation techniques, Purton et al. (1996) obtained lattice strain parameters fitting trace elements partition coefficients for CaO, diopside, orthoenstatite and forsterite. Without a reduced parameter space (especially for E^{M1} for the orthoenstatite), DOUBLE FIT is unable to fit the Ni partition coefficients (Fig. 6a). This demonstrated the limitation of an empirical model, without prior constraints on cation site assignment. Prior determination of the main host cation for each site allows to reduce the parameter space for r_0 and to evaluate each E, and guarantees a more accurate fit.

Finally, when many assumptions and constraints are applied to the lattice strain fitting methods, even with data close to chemical equilibrium (Cartier et al., 2014), extreme values can be obtained, especially for r_0^{M2} and D_0^{M2}. For instance, Cartier et al. (2014) obtained very low r_0^{M2} for 3+ cations (0.66 to 0.79; Fig. 6b), which would imply the absence of Ca and other large cations in the M2 site. In fact, the radius of the M2 site in orthopyroxene is generally around 0.81–0.87 in this range of composition, i.e. Ca + Na + Mn = 0.15–1.1 wt% with Ca > Na >> Mn (Cameron and Papike, 1981). When the same dataset is fit with DOUBLE FIT, only very incompatible cations do not obey the lattice strain model, and best-fit lattice strain parameters (Fig. 6b) are more comparable to other orthopyroxene/melt partitioning studies (i.e. Dalou et al., 2012; Frei et al., 2009).

Conclusions

DOUBLE FIT applies a differential evolutionary algorithm (Storn and Price, 1997) to solve the lattice strain model for two crystal sites when a limited number of experimental data are available. It is the fastest program to date applied to this model. It is designed to be user friendly and easily accessible for users with no prior coding experience.

Acknowledgements

Comments by Jon Blundy, Axel Liebcher and Wim van Westrenen greatly improved the quality and clarity of the manuscript. CD and RD warmly thank Cédric Détry for his contribution and Céline Baudouin for being the first user of DOUBLE FIT and for her priceless discussions, which helped to fix bugs and improve the flexibility and practicality of the program. This work was funded by ANR SlabFlux ANR09BLAN0338 and French Government Laboratory of Excellence initiative n°ANR-10- LABX-0006, the Région Auvergne and the European Regional Development Fund. This is Laboratory of Excellence ClerVolc contribution number 292.

439 **References**

440

441 Adam, J., Green T., 2003. The influence of pressure, mineral composition and water on
442 trace element partitioning between clinopyroxene, amphibole and basanitic melts.
443 European Journal of Mineralogy 15, 831-841.
444 Adam, J., Green T., 2006. Trace element partitioning between mica and amphibole-
445 bearing garnet lherzolite and hydrous basanitic melt: 1. Experimental results and the
446 investigation of controls on partitioning behavior. Contributions to Mineralogy and
447 Petrology 152, 1-17.
448 Aigner-Torres, M., Blundy, J., Ulmer, P., and Pettke, T., 2007. Laser ablation ICPMS
449 study of trace element partitioning between plagioclase and basaltic melts: an
450 experimental approach. Contributions to Mineralogy and Petrology, 153(6), 647-
451 667.
452 Beattie, P., 1994. Systematics and energetics of trace-element partitioning between
453 olivine and silicate melts: Implications for the nature of mineral/melt partitioning.
454 Implications for the nature of mineral/melt partitioning. Chemical Geology 117, 57-
455 71.
456 Bédard, J.H., 2007. Trace element partitioning coefficients between silicate melts and
457 orthopyroxene: parameterizations of D variations. Chemical Geology 244, 263-303.
458 Bédard, J. H. (2014). Parameterizations of calcic clinopyroxene—Melt trace element
459 partition coefficients. Geochemistry, Geophysics, Geosystems, 15(2), 303-336.
460 Bindeman, I. N., Davis, A. M., Drake, M. J., 1998. Ion microprobe study of plagioclase-
461 basalt partition experiments at natural concentration levels of trace elements.
462 Geochim Cosmochim Acta 62, 1175-1193.
463 Blundy, J. D., Wood, B. J., 1991. Crystal-chemical controls on the partitioning of Sr and
464 Ba between plagioclase feldspar silicate melts and hydrothermal solutions.
465 Geochimica et Cosmochimica Acta 55, 193-209.
466 Blundy, J. D., Wood B. J., 1994. Prediction of crystal-melt partition coefficients from
467 elastic moduli. Nature 372, 452–454.
468 Blundy, J. D., Wood B. J., 2003. Partitioning of trace elements between crystals and
469 melts. Earth and Planetary Science Letters 210(3-4), 383-397.

Bobrov, A. V., Litvin, Y. A., Kuzyura, A. V., Dymshits, A. M., Jeffries, T., Bindi, L. 2014. Partitioning of trace elements between Na-bearing majoritic garnet and melt at 8.5 GPa and 1500–1900 C. Lithos, 189, 159-166.

Brenan, J. M., Shaw H. F., Ryerson F. J., Phinney D. L., 1995. Experimental determination of trace element partitioning between pargasitic amphibole and synthetic hydrous melt. Earth and Planetary Science Letters 135, 1-11.

Brice, J. C., 1975. Some thermondynamic aspects of strained crystals. Journal of Crystal Growth 28, 249-253.

Cartier, C., Hammouda, T., Doucelance, R., Boyet, M., Devidal, J. L., Moine, B., 2014. Experimental study of trace element partitioning between enstatite and melt in enstatite chondrites at low oxygen fugacities and 5 GPa. Geochimica et Cosmochimica Acta, 130, 167-187.

Corgne, A., Wood, B. J., 2004. Trace element partitioning between majoritic garnet and silicate melt at 25 GPa. Physics of the Earth and Planetary Interiors, 143, 407-419.

Dalou, C., Koga, K. T., Hammouda, T., Poitrasson, F., 2009. Trace element partitioning between carbonatitic melts and mantle transition zone minerals: Implications for the source of carbonatites. Geochimica et Cosmochimica Acta, 73(1), 239-255.

Dalou, C., Koga, K. T., Shimizu, N., Boulon J., Devidal J. L., 2012. Experimental determination of F and Cl partitioning between lherzolite and basaltic melt. Contributions to Mineralogy and Petrology 163, 591-609.

Dalpé C., Baker D. R., 2000. Experimental investigation of large-ion lithophile-element, high-field-strength-element, and rare-earth-element partitioning between calcic amphibole and basaltic melt: the effects of pressure and oxygen fugacity. Contributions to Mineralogy and Petrology, 140, 233-250.

Dygert, N., Liang, Y., Sun, C., Hess, P., 2014. An experimental study of trace element partitioning between augite and Fe-rich basalts. Geochimica et Cosmochimica Acta, 132, 170-186.

Frei, D., Liebscher, A., Wittenberg, A., Shaw, C. S., 2003. Crystal chemical controls on rare earth element partitioning between epidote-group minerals and melts: an experimental and theoretical study. Contributions to Mineralogy and Petrology 146(2), 192-204.

Frei, D., Liebscher, A., Franz, G., Wunder, B., Klemme, S., Blundy, J. D., 2009. Trace element partitioning between orthopyroxene and anhydrous silicate melt on the lherzolite solidus from 1.1 to 3.2 GPa and 1,230 to 1,535°C in the model system Na_2O - CaO - MgO - Al_2O_3 - SiO_2. Contributions to Mineralogy and Petrology 157, 473-490.

Gaetani, G. A., Kent, A. J. R., Grove, T. L., Hutcheon, I. D., Stolper, E. M., 2003. Mineral/melt partitioning of trace elements during hydrous peridotite partial melting. Contributions to Mineralogy and Petrology 145, 391-405.

Green, T. H., Blundy, J. D., Adam J., Yaxley, G. M., 2000. SIMS determination of trace element partition coefficients between garnet, clinopyroxene and hydrous basaltic liquids at 2 - 7.5 GPa and 1080 – 1200ºC. Lithos 53,165-187.

Hill, E., Wood, B. J., Blundy, J. D., 2000. The effect of Ca-Tschermaks component on trace element partitioning between clinopyroxene and silicate melt. Lithos 53, 203-215.

Klemme, S., Blundy, J. D., Wood, B. J., 2002. Experimental constraints on major and trace element partitioning during partial melting of eclogite. Geochimica et Cosmochimica Acta 6(17), 3109-3123.

La Tourrette, T., Hervig, R. L., Holloway, J. R., 1995. Trace element partitioning between amphibole phlogopite and basanite melt. Earth and Planetary Science Letters. 135, 13-30.

Lee, C. T. A., Harbert, A., Leeman, W. P., 2007. Extension of lattice strain theory to mineral/mineral rare-earth element partitioning: an approach for assessing disequilibrium and developing internally consistent partition coefficients between olivine, orthopyroxene, clinopyroxene and basaltic melt. Geochimica et Cosmochimica Acta, 71(2), 481-496.

McDade, P., Blundy, J. D., Wood, B. J., 2003a. Trace element partitioning between mantle wedge peridotite and hydrous MgO-rich melt. American Mineralogist 88, 1825-1831.

McDade, P., Blundy, J. D., Wood, B. J., 2003b. Trace element partitioning on the Tinaquillo Lherzolite solidus at 1.5 GPa. Physics of the Earth and Planetary Interiors 139, 129-147.

Michely, L. T., Leitzke, F. P., Speelmanns, I. M., Fonseca, R. O. C., 2017. Competing effects of crystal chemistry and silicate melt composition on trace element behavior in magmatic systems: insights from crystal/silicate melt partitioning of the REE, HFSE, Sn, In, Ga, Ba, Pt and Rh. Contributions to Mineralogy and Petrology, 172(6), 39.

Nagasawa, H., 1966. Trace element partition coefficient in ionic crystals. Science 152, 767-769.

Onuma, N., Higuchi, H., Wakita, H., Nagasawa, H., 1968. Trace element partitioning between two pyroxenes and the host lava. Earth and Planetary Science Letters 5, 47-51.

Pertermann, M., Hirschmann, M. M., Hametner, K., Günther, D., Schmidt, M. W., 2004. Experimental determination of trace element partitioning between garnet and silica-rich liquid during anhydrous partial melting of MORB-like eclogite. Geochemistry Geophysics Geosystems G^3 5(5), 1-23.

Press, W. H., Teukolsky, S. A., Vetterling, W. T., Flannery, B. P., 1992. Numerical Recipes in C. Cambridge: 2nd edn, Cambridge University Press.

Purton, J. A., Allan, N. L., Blundy, J. D., Wasserman, E. A., 1996. Isovalent trace element partitioning between minerals and melts: a computer simulation study. Geochimica et Cosmochimica Acta, 60(24), 4977-4987.

Shannon, R. D. 1976. Revised effective ionic radii and systematic studies of interatomic distances in halides and chalcogenides. Acta Crystallographica A32, 751-767.

Storn, R., Price, K. 1997. Differential evolution - A simple and efficient heuristic for global optimization over continuous spaces. Journal of Global Optimization 11, 341-359.

Sun, C., Graff, M., Liang, Y., 2017. Trace element partitioning between plagioclase and silicate melt: the importance of temperature and plagioclase composition with implications for terrestrial and lunar magmatism. Geochimica et Cosmochimica Acta 206, 273-295

Taura, H., Yurimoto, H., Kurita, K., Sueno, S., 1998. Pressure dependence on partition coefficients for trace elements between olivine and the coexisting melts." Physics and Chemistry of Minerals 25, 469-484.

563 Tiepolo, M., Oberti, R., Zanetti, A., Vannucci, R., and Foley, S.F., 2007. Trace-element
564 partitioning between amphibole and silicate melt. Reviews in Mineralogy and
565 Geochemistry, 67(1), 417-452.
566 Tepley, F. J., Lundstrom, C. C., McDonough, W. F., Thompson, A., 2010. Trace element
567 partitioning between high-An plagioclase and basaltic to basaltic andesite melt at 1
568 atmosphere pressure. Lithos 118, 82-94
569 van Kan Parker, M., Liebscher, A., Frei, D., van Sijl, J., van Westrenen, W., Blundy, J.,
570 Franz, G., 2010. Experimental and computational study of trace element distribution
571 between orthopyroxene and anhydrous silicate melt: substitution mechanisms and
572 the effect of iron. Contributions to Mineralogy and Petrology 159, 459-473.
573 van Westrenen, W., Blundy, J. D., Wood, B. J., 1999. Crystal-chemical controls on trace
574 element partitioning between garnet and anhydrous silicate melt. American
575 Mineralogist 84, 838-847.
576 van Westrenen, W., Blundy, J. D., Wood, B. J., 2000a. Atomistic simulation of trace
577 element incorporation into garnets - comparison with experimental garnet-melt
578 partitioning data. Geochemica et Cosmochemica Acta 64, 1629-1639.
579 van Westrenen, W., Blundy, J. D., Wood, B. J., 2000b. Effect of Fe^{2+} on garnet-melt trace
580 element partitioning: experiments in FCMAS and quantification of crystal-chemical
581 controls in natural systems. Lithos 53, 189-201.
582 Wood, B. J., Blundy, J. D., 1997. A predictive model for rare earth element partitioning
583 between clinopyroxene and anhydrous silicate melt. Contributions to Mineralogy
584 and Petrology 129, 166-181.
585 Wood, B. J., Blundy, J. D., Robinson, J. A. C., 1999. The role of clinopyroxene in
586 generating U-series disequilibrium during mantle melting. Geochemica et
587 Cosmochemica Acta 63, 1613-1620.
588 Zanetti, A., Tiepolo, M., Oberti, R., Vannucci, R., 2004. Trace-element partitioning in
589 olivine: modelling of a complete data set from a synthetic hydrous basanite melt.
590 Lithos 75, 39-54.
591
592
593

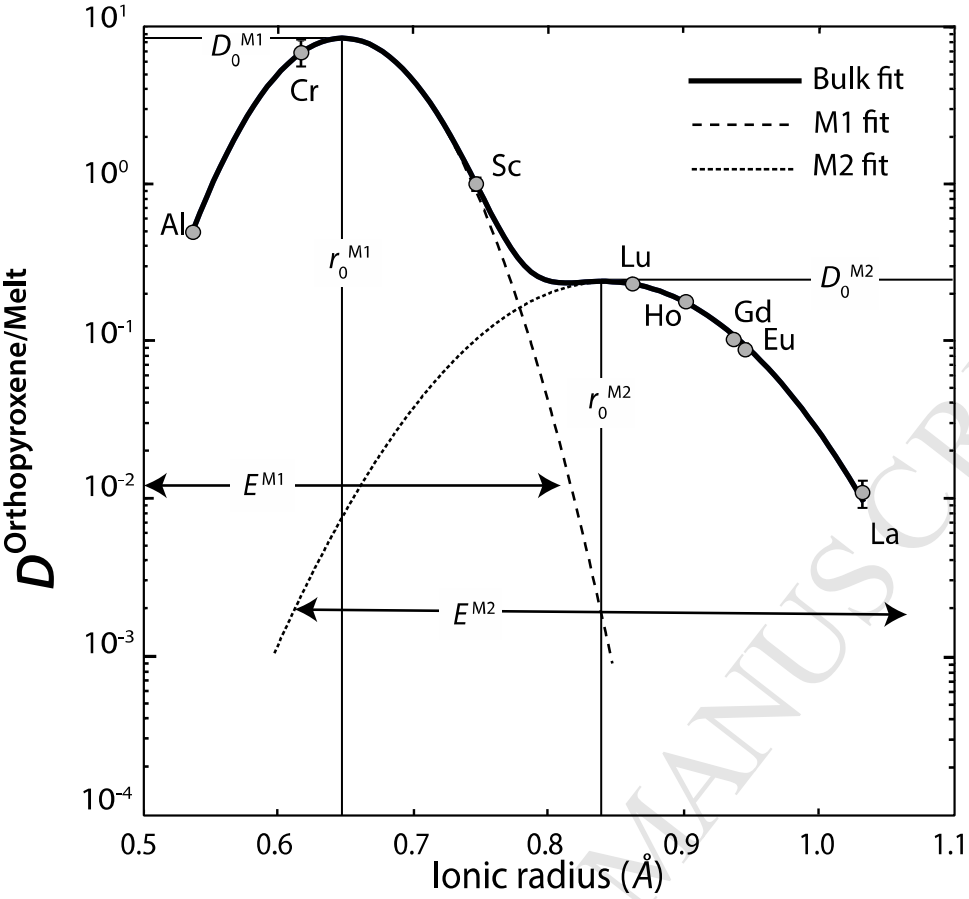

Figure 1: Example of the lattice strain model applied to experimentally determined partition coefficients between orthopyroxene and a basaltic melt for trivalent cations (sample F4p#3a, Dalou et al., 2012). The solid curve represents the fit of the lattice-strain model to $D_i^{Opx/melt}$, i.e. the sum of $D_i^{M1/melt}$ (dotted parabola) and $D_i^{M2/melt}$ (dashed parabola). Circles represent measured $D_i^{Opx/melt}$, i.e. the concentration of element *i* in orthopyroxene (opx) over the concentration of the same element in the equilibrated melt.

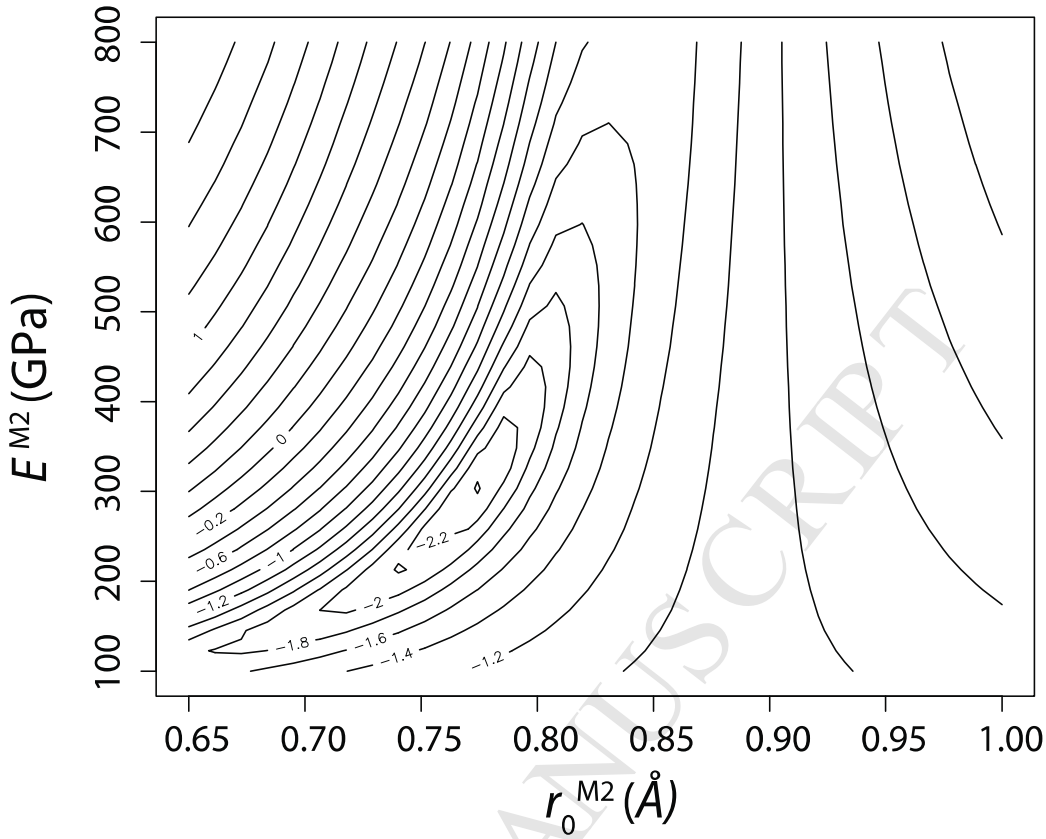

Figure 2: Contour plot of the uncertainty-weighted residual square surface of E_0^{M2} versus r_0^{M2}. To illustrate the subtle structure, the log of the residual value is shown:

$$\log(s^2) = \log\left(\frac{\Sigma\left(\left.\left(ln\left(D^i_{observed}\right) - ln\left(D^i_{modelled}\right)\right)\right/ \delta^i_D\right)^2}{\Sigma\left(\left.1\right/ \delta^i_D\right)^2}\right).$$

Note the presence of two small local minima, as well as the change of the gradient at around r_0^{M2} = 0.9. Because there are six parameters to solve for, it is impossible to visualize the true residual surface in a 2-D plot. The plot shown here is chosen to illustrate our point by picking a plane passing through the true global minimum of the mapped area. The two most varying parameters were chosen to define the plane.

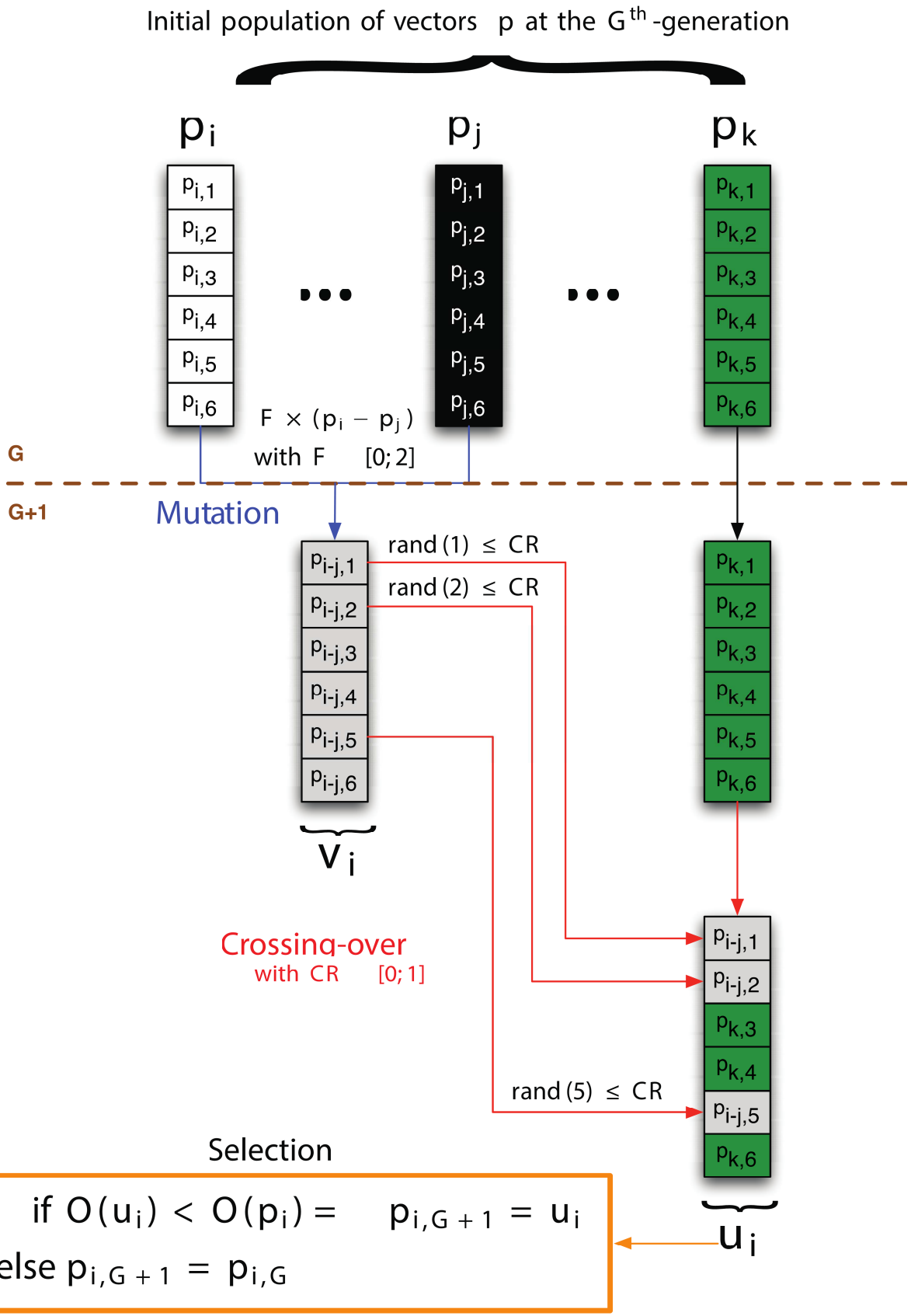

Figure 3: Illustration of the mutation, cross-over, and selection processes of the differential evolutionary algorithm for **p** = 6 parameters. See text for details.

ORTHOPYROXENE_example.csv

Ri	D	eD
1.032	0.003	0.001
0.947	0.026	0.001
0.938	0.048	0.001
0.901	0.102	0.002
0.861	0.187	0.004
0.745	0.873	0.009
0.615	5.606	0.042
0.535	0.374	0.032

CLINOPYROXENE_example.csv

Ri	D	eD
1.016	0.054	0.018
1.066	0.273	0.006
1.053	0.323	0.027
1.015	0.467	0.006
0.977	0.461	0.010
0.745	1.213	0.017
0.615	6.543	0.020
0.535	0.376	0.173

OLIVINE_example.csv

Ri	D	eD
0.947	0.003	0.001
0.938	0.006	0.003
0.901	0.013	0.004
0.861	0.033	0.004
0.745	0.196	0.013
0.535	0.004	0.001

GARNET_example.csv

Ri	D	eD
1.016	0.001	0.001
1.066	0.288	0.024
1.053	0.573	0.044
1.015	2.369	0.502
0.977	5.822	0.502
0.870	6.904	0.165

Figure 4: Example of the required data file format applied to orthopyroxene, clinopyroxene, olivine, and garnet. Note that no assumption is made in the data file of the location (M1 or M2 site) of the cations.

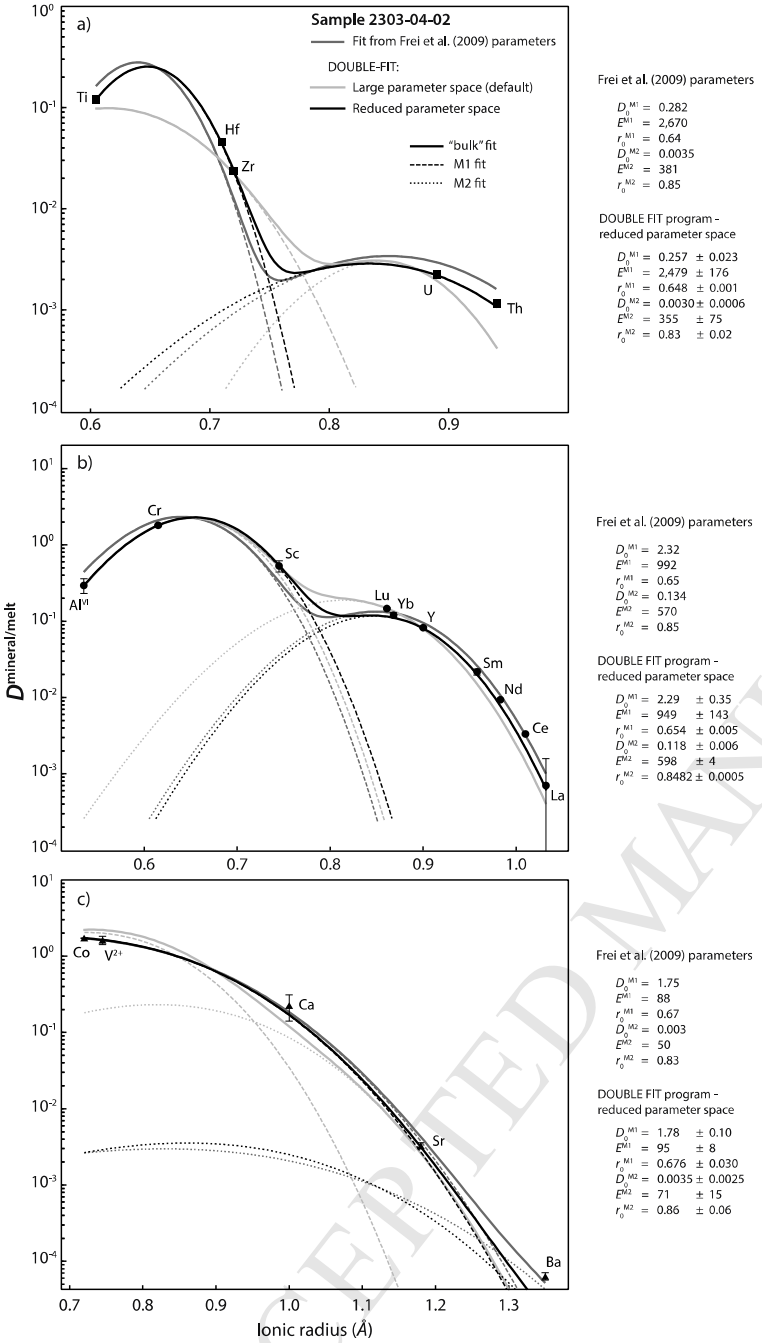

Figure 5: Example results of the DOUBLE FIT program using orthopyroxene/melt partitioning data of sample 2303-04-02 (Frei et al., 2009) for a) tetravalent cations, b) trivalent cations, and c) divalent cations. Depending on the size of the parameter space, DOUBLE FIT gives different results. With a reduced parameter space (D_0^{M1}min = 0.15, E^{M1}min = 2000, and E^{M2}max = 500), DOUBLE FIT fits the lattice strain model with five points for the tetravalent cations. However, with only Ba in the M2 site, DOUBLE FIT cannot properly fit the divalent data even when constrained with $D_0^{M2} \in [0.001 ; 0.01]$ $E^{M2} \in [30 ; 100]$ GPa)

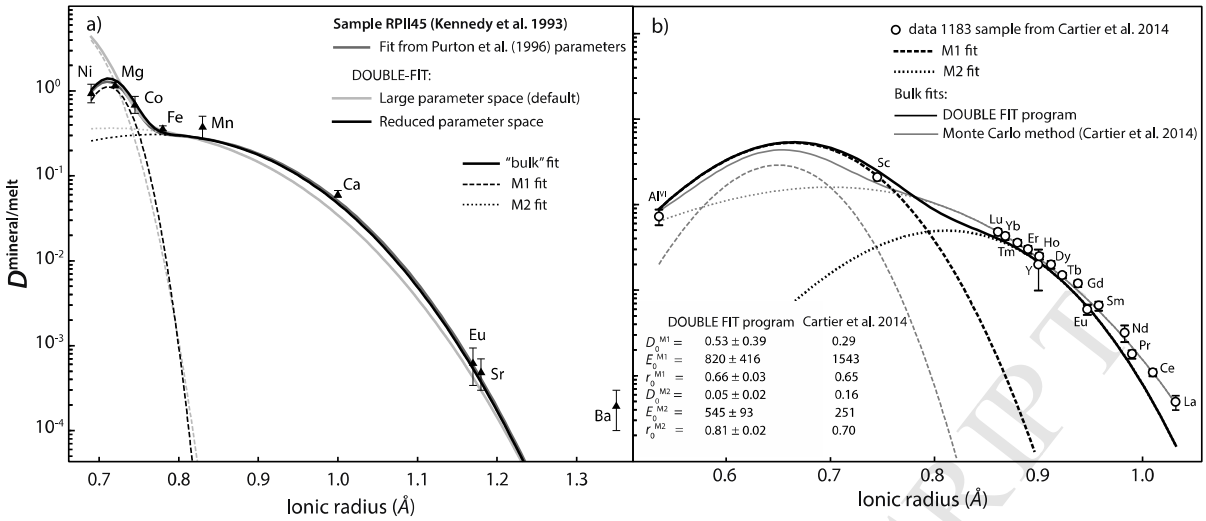

Figure 6: Comparison of the empirical fit of DOUBLE FIT (black curves) with methods fitting parameters a) E and r_0 (Purton et al. 1996), and b) E^{M1} and E^{M2} (Cartier et al. 2014) based on the energetics of ion substitution (dark grey curves in (a) and (b)). Cartier et al. (2014) determined D_0 and r_0 for the M1 and M2 sites by a Monte Carlo method. Light grey curves shows DOUBLE FIT model using the default parameter space.

- DOUBLE FIT applies to solve the lattice strain model for two crystal sites mineral.
- It uses a differential evolutionary algorithm (Storn and Price, 1997).
- It works even when a limited number of experimental data are available.
- It is the fastest program to date applied to this model.
- It is designed to be user friendly for users with no prior coding experience.